

## A Ferrocene–Peptide Conjugate as a Hydrogenase Model System

Xavier de Hatten,<sup>[a,bl]</sup> Eberhardt Bothe,<sup>[cl]</sup> Klaus Merz,<sup>[al]</sup> Ivan Huc,<sup>[bl]</sup> and Nils Metzler-Nolte\*<sup>[al]</sup>*Dedicated to Prof. B. Krebs on the occasion of his 70th birthday***Keywords:** Bioorganometallic chemistry / Cofactors / Enzyme models / Metallocenes / Hydrogenase / Peptides / Spectro-electrochemistry

This work introduces a bis(cysteine) ligand to build a small peptidic model system of hydrogenase enzymes.  $\text{Fe}(\text{C}_5\text{H}_4\text{CO-Cys-OMe})_2$  ( $\text{LH}_2$ ) has been employed as a chelate for an iron–carbonyl complex, which mimics two essential structural properties of the hydrogenase class of enzymes, namely the coordination of the iron–carbonyl core to peptide ligands and the presence of an electrochemical relay in spatial proximity. The treatment of  $\text{LH}_2$  with  $\text{Fe}_3(\text{CO})_{12}$  yields  $\text{LFe}_2(\text{CO})_6$  (**3a**), which is the first peptide-coordinated iron hydrogenase active-site model complex. Compound **3a** was fully characterized spectroscopically ( $^1\text{H}$  NMR,  $^{13}\text{C}$  NMR, IR and Mössbauer spectroscopy, mass spectrometry and elemental analysis). A single-crystal X-ray analysis con-

firms the proposed structure and reveals a staggered conformation of the  $\text{Fe}_2(\text{CO})_6\text{S}_2$  core. Fourier transform infrared (FTIR) spectroelectrochemistry reveals an electronic interaction between the peptide backbone and the iron–carbonyl cluster, but not with the ferrocene subsite. The introduction of this peptidic cysteine-based ligand into hydrogenase model chemistry helps to confirm the proposed cofactor biosynthesis and understand the electronic interplay between the metal–carbonyl active site and the protein environment in this important class of enzymes.

(© Wiley-VCH Verlag GmbH & Co. KGaA, 69451 Weinheim, Germany, 2008)

**Introduction**

Hydrogenase enzymes ( $\text{H}_2$ ases) catalyze the reversible splitting of dihydrogen into protons and electrons. This interesting and highly efficient class of enzymes was discovered 77 years ago.<sup>[1]</sup> In the vast majority of these enzymes, catalytic dihydrogen conversion occurs at a bimetallic (NiFe or FeFe) site, in which the Fe atoms are coordinated to carbonyl (CO) and cyanide ( $\text{CN}^-$ ) ligands.<sup>[2–4]</sup> Electron transfer to or from the active site is achieved through a series of FeS clusters.  $\text{H}_2$ ase enzymes have sparked considerable research interest due to the pressing energy problems of today's developed world.<sup>[5]</sup> In  $\text{H}_2$ ase model chemistry small structural models are sought to achieve a better understanding of the mechanistic details of  $\text{H}_2$  production.<sup>[6]</sup> Besides, it is hoped that a functional model of

these enzymes may enable the development of electrocatalytic materials for the efficient synthetic production of  $\text{H}_2$ . Accordingly, there is an urge to develop small, well-defined, easy-to-synthesize and active “free-standing” analogues of  $\text{H}_2$ ase enzymes.

Several groups have developed different approaches to this challenging task<sup>[7–13]</sup> and structural models of the bimetallic Fe-only  $\text{H}_2$ ase active site, in particular, have matured considerably in recent years.<sup>[14–16]</sup> Elucidation of the catalytic mechanism, especially the identification and location of hydride intermediates, has been a focus in recent work.<sup>[17–21]</sup> To this end, diiron model compounds or even ruthenium complexes (for which no natural precedent exists) with a variety of unnatural ligands such as phosphanes and carbenes have been employed.<sup>[18,19,22,23]</sup> Other examples have reported attachment of the active-site cluster models to electrochemical sensors such as porphyrins,<sup>[24]</sup> a ruthenium-based photosensitizer<sup>[25–27]</sup> or even models of the natural  $[\text{Fe}_4\text{S}_4]$  cubane unit.<sup>[28]</sup> In the bimetallic [NiFe]  $\text{H}_2$ ase, the Ni atom is coordinated to four sulfur atoms from cysteine amino acids, two of which bridge the Fe atom. These four cysteines are the only proteinogenic ligands coordinating the two metal centres. Given this fact, and the multitude of model complexes highlighted above, it is as-

[a] Faculty of Chemistry and Biochemistry, Inorganic Chemistry I – Bioinorganic Chemistry, Universitätsstraße 150, 44801 Bochum, Germany  
Fax: +49-234-32-14378  
E-mail: Nils.Metzler-Nolte@rub.de

[b] Université de Bordeaux I – CNRS UMR 5248, Institut Européen de Chimie et de Biologie, 2, rue Robert Escarpit, 33607 Pessac, France

[c] Max-Planck-Institute for Bioinorganic Chemistry, Stiftstr. 34-36, 45470 Mülheim an der Ruhr, Germany

tonishing how little attention has been devoted to mimicking the *peptide environment* in H<sub>2</sub>ase model systems. Only one example in the literature employs the naturally occurring amino acid cysteine as a ligand for an iron–carbonyl core.<sup>[29]</sup> In this particular case an unexpected rearrangement of the cysteine carbon skeleton occurs, which is not observed in the naturally occurring hydrogenases. This finding is therefore somewhat at odds with the current model of metal–carbonyl cofactor biosynthesis. Moreover, certain interactions between the metal centres and the coordinating amino acids may be crucial for spectroscopic features and the striking activity of these enzymes. Evidently, such crucial interactions will not be detected in model compounds with the unnatural ligands described above.

In an effort towards more realistic, peptide-based H<sub>2</sub>ase model compounds, we report herein the covalent attachment of a diiron–hexacarbonyl core to two cysteine molecules that are connected via peptide bonds to a ferrocene (dicyclopentadienyl iron, Cp<sub>2</sub>Fe) moiety. This compound mimics two key features of the H<sub>2</sub>ase active site, namely, exclusive coordination to biologically occurring ligands (Cys) and the close spatial proximity of an electrochemically active scaffold (ferrocene). It also allows us to scrutinize the electronic interactions between the iron–carbonyl core and the peptide environment.

## Results and Discussion

We have previously reported that the S-protected ferrocenoyl dicysteine, Fe[C<sub>5</sub>H<sub>4</sub>CO–Cys(Trt)–OMe]<sub>2</sub> (**1**; Scheme 1), may be prepared by standard peptide coupling procedures.<sup>[30]</sup> The trityl (Trt) protecting group was subsequently removed with TFA (trifluoroacetic acid) in the presence of phenol, which suppresses the acid-catalyzed oxidative degradation of ferrocene. The dithiol derivative Fe[C<sub>5</sub>H<sub>4</sub>–CO–Cys(H)–OMe]<sub>2</sub> (**2**) thus obtained reacts with Fe<sub>3</sub>(CO)<sub>12</sub> to give the dithiolato-bridged diiron–hexacarbonyl H<sub>2</sub>ase subsite mimic **3a** (Scheme 1). A small amount of the disulfide-bridged derivative **3b** is obtained from this reaction but is readily separated from **3a** by column chromatography. Compound **3b** has previously been reported by Kraatz et al. and was thus identified by comparison of its spectroscopic data.<sup>[31]</sup> All of the complexes **1**, **2**, **3a** and **3b** were characterized by standard spectroscopic methods, including <sup>1</sup>H NMR, <sup>13</sup>C NMR, UV and IR spectroscopy, FAB-MS and elemental analysis. All analytical data confirm the proposed structures. Compound **3a** was further characterized by electrochemistry, FTIR spectroelectrochemistry, Mössbauer spectroscopy and single-crystal X-ray crystallography.

The FAB-MS spectrum of **3a** shows a peak envelope centred at *m/z* = 786.9 with an isotope pattern that matches the proposed structure, in particular the presence of three iron atoms. However, the base peak is observed at *m/z* = 617.9 (100%), which corresponds to the loss of six CO ligands of the iron–carbonyl core of **3a**. The presence of the metal–carbonyl groups is corroborated by their <sup>13</sup>C NMR

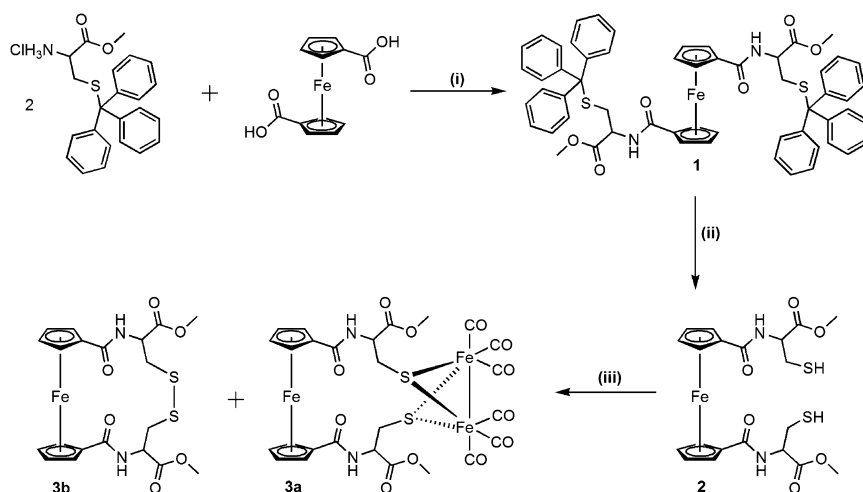
signals around 208 ppm. Compound **3a** is diamagnetic, which is consistent with an Fe<sup>II</sup> ferrocene centre and a low-spin Fe(I)<sub>2</sub>(CO)<sub>6</sub> core. This assignment is further supported by the solid-state Mössbauer spectrum of **3a** at 80 K, which can readily be simulated as a linear combination of two overlapping quadrupole-split doublets (see Figure 1). The isomer shift ( $\delta$ ) and quadrupole splitting ( $\Delta E_Q$ ) parameters (in mm s<sup>-1</sup>) are consistent with two different iron sites in a 1:2 ratio, the first one being associated with the [Cp<sub>2</sub>Fe] subsite ( $\delta$  = 0.512,  $\Delta E_Q$  = 2.295)<sup>[32,33]</sup> and the second with the [Fe<sub>2</sub>CO<sub>6</sub>] subsite ( $\delta$  = 0.045,  $\Delta E_Q$  = 0.893). These latter values are within the range of previous studies on the iron–sulfur cluster-free hydrogenase from methanogenic archaea ( $\delta$  = 0.04,  $\Delta E_Q$  = 0.65).<sup>[34]</sup> The IR spectrum of **3a** in dichloromethane shows three metal–carbonyl stretching bands in the metal–CO region at 2077, 2040 and 2000 cm<sup>-1</sup> (Table 2), which correlate well with the published values of Fe<sub>2</sub>(CO)<sub>6</sub>-(thiolato)<sub>2</sub> compounds,<sup>[10,24,35–37]</sup> and furthermore are similar to the values obtained by Happe et al. on the H<sub>2</sub>ase enzyme of *Chromatium vinosum*.<sup>[38]</sup>

The solid-state structure of **3a** has been determined by single-crystal X-ray diffraction and is shown in Figure 2. The two sulfur atoms bridge both iron centres of the iron–carbonyl core, creating an open butterfly Fe<sub>2</sub>S<sub>2</sub> cluster. The Fe(CO)<sub>3</sub> subunits are in a staggered conformation. Inclusion of the ferrocene moiety results in the formation of a 14-membered macrocycle made up of two iron atoms, two sulfur and two nitrogen atoms and eight carbon atoms. The substitution pattern of the ferrocene is in a nearly perfect 1,2' conformation with *M*-helical chirality.<sup>[39]</sup> However, CD spectroscopy in dichloromethane does not show a strong negative band around 450 nm as is usually the case in 1,2'-substituted ferrocenoyl peptides.<sup>[40,41]</sup> In contrast to earlier studies, there is no intramolecular hydrogen bond to stabilize the helical form of **3a**. Consequently, the molecule is more flexible in solution and the helical handedness is much less pronounced in solution than in the hydrogen-bonded structures of previous work.

As shown in Table 1, the metrical parameters of the iron–carbonyl core of **3a** are in good agreement with the parameters obtained from the crystal structures of Fe-only H<sub>2</sub>ases from *Desulfovibrio desulfuricans*<sup>[3]</sup> and *Clostridium pasteurianum*.<sup>[2]</sup> The structural similarity between **3a** and the naturally observed structures is reassuring although the bridging dithiolate ligand used here is not of the propanedithiolate/bis(methylthiol)amine type found in the Fe-only H<sub>2</sub>ase active site, but rather related to the cysteinyl residues observed in the [NiFe] H<sub>2</sub>ase active site.<sup>[42]</sup>

We have investigated the spectroscopic changes of different parts of **3a** upon electrochemical oxidation and reduction in order to elucidate possible electron transfer between the iron–carbonyl and the ferrocene subsites.

The cyclic voltammogram of **3a** shows two reversible processes (Figure 3a). First, an uncomplicated redox process (low peak separation and peak positions independent of the scan rates) at *E*<sub>1/2</sub> = 433 mV vs. Cp<sub>2</sub>Fe/Cp<sub>2</sub>Fe<sup>+</sup> is assigned to the reversible Fe<sup>II</sup>/Fe<sup>III</sup> oxidation of the ferrocene moiety, which exhibits an undisturbed one-electron



Scheme 1. Synthesis of  $\text{Fe}[\text{C}_5\text{H}_4\text{-CO-Cys-OMe}]_2[\text{Fe}_2(\text{CO})_6]$  (**3a**). Reagents and conditions: (i) TBTU, DIEA; (ii) TFA, phenol, TIS; (iii)  $\text{Fe}_3(\text{CO})_{12}$ . See Experimental Section for details.

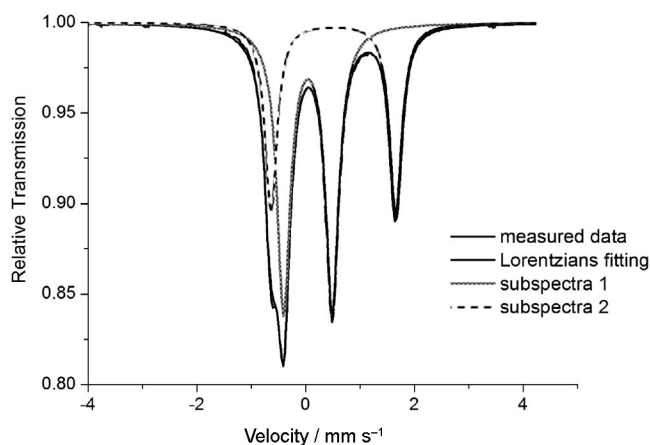


Figure 1. Mössbauer spectrum of **3a**, recorded at 80 K as a solid sample.

transfer under almost all circumstances.<sup>[43]</sup> For the reduction process around ca  $-1.3$  V vs.  $\text{Cp}_2\text{Fe}/\text{Cp}_2\text{Fe}^+$  the two peaks of the wave are separated by almost 0.5 V, with higher peak separations at higher scan rates. This behaviour is typical for sluggish heterogeneous electron-transfer kinetics, that is, an *electrochemically* quasireversible reaction. However, the symmetry of reduction and subsequent reoxidation seen in the cyclic voltammogram demonstrate the *chemical* reversibility of the process. This is confirmed by the results of spectroelectrochemical studies, *vide infra*. The peak areas for this process are about twice that of the ferrocene-based oxidation waves. This demonstrates that the reduction is a two-electron process, that is, both iron atoms of the iron-carbonyl subunit are reduced simultaneously. One irreversible reduction at  $E_{ac} \approx 0.85$  V vs.  $\text{Cp}_2\text{Fe}/\text{Cp}_2\text{Fe}^+$  is also observed and is assigned to the oxidative degradation of the  $\text{S}_2\text{Fe}_2(\text{CO})_6$  core. During the course of these cyclovoltammetric experiments the three-iron core of the molecule alternates between four oxidation states of iron, which are formally 0, I, II and III.

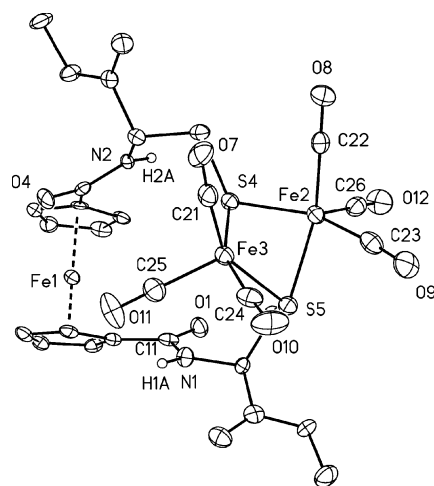


Figure 2. ORTEP drawing of **3a** with thermal ellipsoids at 50% probability level. Hydrogen atoms are omitted for clarity except for NH atoms. Selected bond lengths [Å], angles [°] and dihedral angles [°]: Fe2–Fe3 2.5170(9), Fe2–C22 1.791(5), Fe2–C26 1.814(6), Fe2–C23 1.820(5), Fe3–C21 1.775(6), Fe3–C24 1.791(5), Fe3–C25 1.827(5), Fe1–Cp(centroid) 1.646(4) and 1.637(4), Cp(centroid)–Fe–Cp(centroid) 2.9, C25–Fe3–Fe2–C26  $-8.4$ ; Cp–CO dihedral O4–C16–C8–C7  $31.5$ . Further bond lengths and angles are given in Table 1.<sup>[58]</sup>

Table 1. Selected geometrical data of **3a** in comparison to experimental structural data from natural enzyme active sites.

	Fe–Fe [Å]	Fe–S [Å]	Fe–S–Fe [°]	S–Fe–S [°]	S–Fe–S–Fe [°]
<b>3a</b>	2.52	2.24	67.7	80.6	54.9
1HFE <sup>[a]</sup>	2.55	2.27	67.9	81.2	54.0
1FEH <sup>[b]</sup>	2.62	2.32	68.3	82.0	53.4

[a] Measured on the experimental crystallographic data of *Desulfovibrio desulfuricans* iron hydrogenase (RCSB reference 1HFE).<sup>[3]</sup>  
 [b] Measured on the experimental crystallographic data of Fe-only hydrogenase from *Clostridium pasteurianum* (RCSB reference 1FEH).<sup>[2]</sup>

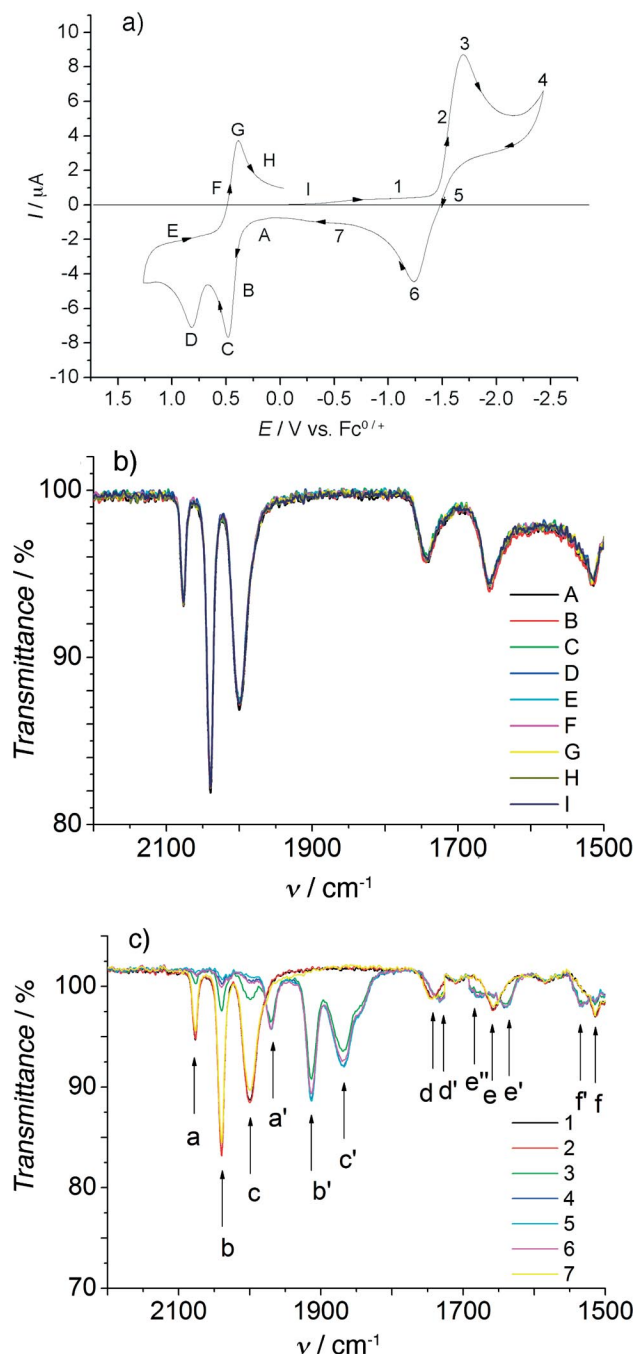


Figure 3. (a) Cyclic voltammogram ( $100 \text{ mV s}^{-1}$ ) of a solution of complex **3a** in  $\text{CH}_3\text{CN}$  containing  $0.1 \text{ M}$   $(\text{Bu})_4\text{NPF}_6$  (potentials are given vs.  $\text{Cp}_2\text{Fe}/\text{Cp}_2\text{Fe}^+$  used as external standard). Solution FTIR spectra between  $1500\text{--}2200 \text{ cm}^{-1}$ , observed during oxidation (b) and reduction (c) of complex **3a**. The spectra were measured while recording a cyclic voltammogram in an optically transparent spectroelectrochemical thin-layer (OTTLE) cell at  $-25^\circ\text{C}$  at a scan rate of  $3 \text{ mV s}^{-1}$ . The potentials at which the (single scan) IR spectra were measured are indicated with letters (Figure 3b) and numbers (Figure 3c) on the cyclic voltammogram (Figure 3a). Unlike in Figure 3a, the current was reverted before decomposition of the material at  $0.8 \text{ V}$  for the experiment described in Figure 3b, effectively making points D and E equal (at  $0.8 \text{ V}$ ).

Single-scan FTIR spectra were recorded between  $2200$  and  $1500 \text{ cm}^{-1}$  during the electrochemical experiment at a low scan rate. All measurements were carried out at  $-25^\circ\text{C}$

to avoid decomposition of the material. For the same reason the electrochemical scan was reversed at  $0.8 \text{ V}$  (see caption for Figure 3). In this region six different IR bands are observed, three relatively strong bands at  $2077$ ,  $2040$  and  $2000 \text{ cm}^{-1}$  assigned to the CO stretching vibrations of the metal–carbonyl ligands of the iron–carbonyl core and three weak bands at  $1743$ ,  $1657$  and  $1516 \text{ cm}^{-1}$ , attributed to the ester carbonyl stretching vibration, the amide carbonyl stretching vibration and the amide bending mode of the peptide, respectively (Table 2).<sup>[44]</sup> The latter two are also frequently referred to as amide I and amide II.

The IR spectra measured during the course of the electrochemical oxidation and reduction of the ferrocenyl moiety of complex **3a** at  $433 \text{ mV}$  (spectra A–I) are shown in Figure 3b. Clearly, ferrocene oxidation does not significantly affect any CO bands with a maximum shift of  $\Delta\tilde{\nu}_{\text{max}} = 3 \text{ cm}^{-1}$ . There is no electron transfer between the ferrocene moiety and the  $\text{Fe}_2(\text{CO})_6$  core, which would result in a shift of the carbonyl bands upon ferrocene oxidation. Furthermore, the peptide bonds are unaffected by the positive charge of the ferrocenium moiety that is in close proximity. This situation is dramatically different when the  $\text{Fe}_2(\text{CO})_6$  core is reduced and reoxidized. Spectra recorded at the start (spectrum 1, Figure 3c) and at the end (spectrum 7, Figure 3c) of the reduction and the reoxidation of the Fe carbonyl core of **3a** show a perfect overlap, thereby confirming full reversibility of the two processes investigated. From the low scan rate ( $3 \text{ mV s}^{-1}$ ) one can estimate that under our experimental conditions (degassed,  $\text{O}_2$ -free solution at  $-25^\circ\text{C}$ ) the oxidized and reduced forms of **3a** persist in solution for at least  $10^3 \text{ s}$ .

It is surprising to note that all six carbonyl vibration and bending bands are shifted upon reduction of **3a** to **3a**<sup>2-</sup>. The carbonyl vibration bands of the iron–carbonyl core a, b, and c are all shifted by more than  $100 \text{ cm}^{-1}$  to lower values becoming a', b' and c' (Table 2). These shifts are expected, as an increase in electron density at the iron centre increases the M–C back-bonding, which results in a bathochromic shift of the C–O vibrational frequency.<sup>[45]</sup> Unexpectedly, however, a significant shift of the peptide backbone CO stretching and bending vibrations was also observed as a result of the reduction of the iron–carbonyl core. The CO bands of the peptide backbone (d, e and f of the starting spectra) are displaced to d', e', e'' and f' with shifts in the range of  $10$  to  $25 \text{ cm}^{-1}$  (Table 2). It seems that the additional charge of **3a**<sup>2-</sup> is partly transferred from the diiron–carbonyl core to the peptide backbone.

In the case of band e, corresponding to the amide bending mode, the band is split during the reduction process (becoming e' and e''), which indicates that the interaction of the reduced metal core with the peptide backbone is asymmetric. A closer inspection of the structure of **3a** in Figure 2 may provide an explanation for this unexpected apparent breaking of symmetry. Although the number of bonds between the diiron core and the carbonyl groups of the peptide backbone are the same for both amide carbonyls, the distances between the centre of mass of the diiron core and the oxygen atom of the amide bond are different,

Table 2. IR shifts measured during the course of the cyclic voltammogram performed on **3a**.

	CO <sup>[a]</sup> <sub>ligand1</sub> [cm <sup>-1</sup> ]	CO <sup>[a]</sup> <sub>ligand2</sub> [cm <sup>-1</sup> ]	CO <sup>[a]</sup> <sub>ligand3</sub> [cm <sup>-1</sup> ]	CO <sup>[b]</sup> <sub>amideI-1</sub> [cm <sup>-1</sup> ]	CO <sup>[b]</sup> <sub>amideI-2</sub> [cm <sup>-1</sup> ]	CO <sup>[b]</sup> <sub>amideII</sub> [cm <sup>-1</sup> ]
<b>3a</b> <sup>[c]</sup>	2077	2040	2000	1745	1658	1515
<b>3a</b> (oxidized) <sup>[d]</sup>	2077	2040	2000	1743	1655	1517
<b>3a</b> (reduced) <sup>[e]</sup>	1970	1914	1868	1733	1680/1640	1535

[a] Carbonyl ligand of the iron–carbonyl core. [b] Amide bands I and II of the peptide backbone. [c] Measured on the slopes B and 2. [d] Measured on the slope G. [e] Measured on the slope 5. See Figure 3 for assignment of potentials to slopes B, G, 2 and 5.

being 4.9 Å for the one and 5.6 Å for the other. At the same time, the distance between the iron atom of the ferrocene moiety to the same carbonyl oxygen atoms is around 3.6 Å in both cases. Taken together, we suggest a “through space” electronic communication between the diiron–hexacarbonyl core and the peptide backbone, in which the reduction of the iron–carbonyl core has a more profound influence on the amide carbonyl band, which is closer in space. However, no electronic interaction is observed between the iron–carbonyl and the ferrocene cores. Clearly, this finding is unexpected and merits further investigations, as such a charge delocalization on the peptide backbone may bear significance for the hydrogenase mechanism.

## Conclusions

We synthesized and characterized the first peptide-coordinated iron hydrogenase active-site model complex. The cysteine amino acids are covalently connected to a ferrocene unit, thereby forming a peptidic macrochelate. Reaction with Fe<sub>3</sub>(CO)<sub>12</sub> readily yields a H<sub>2</sub>ase model compound with peptidic cysteine ligands in good yield. Although this compound is not an atom-identical model of the bimetallic Fe-only H<sub>2</sub>ase H cluster, the key structural features of the iron–carbonyl–sulfur core resemble those of the natural system remarkably well. Recent work suggests an independent, chaperone-assisted biosynthesis of the Fe(CO)<sub>x</sub>(CN)<sub>y</sub> cofactors, which are then inserted into the apoenzyme.<sup>[46–48]</sup> Our work confirms that such a reaction is indeed feasible for peptide-bound cysteine *without* the carbon skeleton rearrangement that has been reported for free cysteine.<sup>[29]</sup>

On the basis of the structural similarities, this metallo-cene–peptide conjugate enables us to study the electrochemical interaction of the peptide surrounding the active-site cluster. FTIR spectroelectrochemical experiments show a delocalization of the charge of the two-electron redox process located in the iron–carbonyl subsite through the peptide backbone, whereas the reversible one-electron oxidation of ferrocene has no influence at all. This is all the more surprising because the iron atom of ferrocene is even closer to the amide bond than the iron–carbonyl subsite. A charge delocalization similar to the one observed here may contribute to the remarkable, and mechanistically not yet fully understood, activity of H<sub>2</sub>ase enzymes.

The great majority of model compounds in bioinorganic chemistry are coordination compounds with unnatural organic ligands.<sup>[49]</sup> Nature, in contrast, uses only a limited set of naturally occurring amino acids to achieve a remarkable diversity of functional properties in proteins.<sup>[50,51]</sup> It is surprising that the natural amino acids, or small peptides derived thereof, have rarely been used in synthetic metalloenzyme models.<sup>[52–54]</sup> Only a few synthetic oligopeptide assemblies were designed as artificial metalloenzymes to study the spectroscopic features of the metal ion in a more realistic “protein-like” environment.<sup>[53,55,56]</sup> However, detailed studies of these systems are complicated by their size and limited availability. In sharp contrast, very few small-molecule enzyme model compounds have been studied that rely only on amino acids as ligands for the metal centres. This study shows that such model compounds are urgently needed to elucidate all the details of the interaction of the active-site metal centres with the protein environment, which may go beyond the first coordination sphere. We introduce ferrocene–peptide conjugates as suitable model compounds in this work. Given the ease and diversity of peptide synthesis, the system opens the ground for a host of structural modifications and functional studies not only in hydrogenase chemistry but metalloenzyme model systems in general.

## Experimental Section

**General:** All reactions were carried out under an inert atmosphere, and solvents and reagents were dried and distilled under argon prior to use. Elemental analyses were performed with a Foss Heraeus Vario EL Elementar Analysator. Infrared spectra were recorded with a Perkin–Elmer 1600 series FTIR spectrophotometer. NMR spectra were recorded with a Varian 300 Mercury plus spectrometer (<sup>1</sup>H NMR at 300 MHz). Electron impact (EI) and fast atom bombardment (FAB) mass spectra were measured with a Mat 8200 mass spectrometer. UV/Vis spectra were measured with a Varian CARY 100 spectrophotometer. Cyclic voltammograms were recorded in CH<sub>3</sub>CN solutions (ca. 10<sup>-3</sup> mol L<sup>-1</sup>) with 0.1 M NBu<sub>4</sub>PF<sub>6</sub> as supporting electrolytes with an EG & G M 273 A potentiostat with M 270 software, using a Ag/AgNO<sub>3</sub> (0.01 mol L<sup>-1</sup> in AgNO<sub>3</sub>) reference electrode, a glass carbon disc working electrode with a 2-mm-diameter thickness and a Pt wire counter electrode. Ferrocene was added as an internal reference. Thin-layer FTIR spectroelectrochemical measurements were performed by using an OTTL cell, with an optical path length of 0.17 mm, consisting of a Pt grid working electrode, a glassy carbon counter electrode and a Ag wire as a “quasireference electrode”. <sup>57</sup>Fe Mössbauer spectra were recorded with an Oxford Instruments Mössbauer spectrometer in the

constant acceleration mode, by using  $^{57}\text{Co}/\text{Rh}$  as the radiation source. H–Cys(Trt)–OMe was prepared according to a literature procedure<sup>[57]</sup> in 98% yield.  $^1\text{H}$  NMR ( $\text{CDCl}_3$ ):  $\delta$  = 8.58 (br. s, 2 H, NH<sub>2</sub>), 7.45–7.10 (m, 15 H, CH<sub>ar,Trt</sub>), 3.54 (s, 3 H, CH<sub>3,ester</sub>), 3.37 (m, 1 H, CH<sub>α</sub>), 2.92 (m, 2 H, CH<sub>2,β</sub>) ppm.

**Fe[C<sub>5</sub>H<sub>4</sub>–CO–Cys(Trt)–OMe]<sub>2</sub> (1):** TBTU [*o*-(benzotriazol-1-yl)-*N,N,N',N'*-tetramethyluronium tetrafluoroborate, 2.1 mmol, 653.3 mg] and DIEA (diisopropylethylamine, 2 mmol, 772 μL) were added to a stirred suspension of ferrocene 1,1'-dicarboxylic acid (1 mmol, 274 mg) in freshly distilled CH<sub>2</sub>Cl<sub>2</sub> (30 mL), resulting in complete dissolution. The resulting solution was stirred at ambient temperature for 30 min, followed by filtration to remove the unreacted materials. In a separate flask, H–Cys(Trt)–OMe, HCl (2 mmol, 825 mg) was suspended in distilled CH<sub>2</sub>Cl<sub>2</sub> (20 mL), after which DIEA (2 mmol, 772 μL) was added. The activated carboxylic acid solution was subsequently transferred to the amino acid by a stainless steel cannula at 0 °C mediated with an overpressure of nitrogen. The resulting mixture was stirred overnight at room temperature. The reaction mixture was subsequently diluted to 100 mL with CH<sub>2</sub>Cl<sub>2</sub> and washed consecutively with distilled water (50 mL), HCl (0.1 M, 50 mL), distilled water (50 mL), saturated NaHCO<sub>3</sub> (50 mL) and distilled water (50 mL). The organic phase was dried with MgSO<sub>4</sub>, filtered and the solvent removed by rotary evaporation. The residue was chromatographed on silica gel (EtOAc/hexane, 1:4) to yield **1** as an orange solid (715 mg, 72%). C<sub>58</sub>H<sub>52</sub>FeN<sub>2</sub>O<sub>6</sub>S<sub>2</sub> (993.02): calcd. C 70.15, H 5.28, N 2.82; found C 69.82, H 5.21, N 2.71. MS (EI):  $m/z$  = 993 [M]<sup>+</sup>, 750 [M – Trt]<sup>+</sup>. FTIR (KBr):  $\tilde{\nu}$  = 3326 (br., ν<sub>NH</sub>), 3056–2925 (ν<sub>OH</sub> and ν<sub>CH,Bzl</sub>), 1781 (s, ν<sub>C=O,ester</sub>), 1740 (s, ν<sub>amide stretch</sub>), 1653 (s, ν<sub>amide bending</sub>) cm<sup>-1</sup>.  $^1\text{H}$  NMR ( $\text{CDCl}_3$ ):  $\delta$  = 7.47 (d,  $J_{\text{HH}}$  = 8.3 Hz, 2 H, NH), 7.37–7.20 (m, 30 H, CH<sub>ar,Trt</sub>), 4.83 (m, 2 H, CH<sub>Cp,o</sub>), 4.73 (m, 4 H, CH<sub>α</sub> and CH<sub>Cp,o</sub>), 4.50 (m, 2 H, CH<sub>Cp,m</sub>), 4.34 (m, 2 H, CH<sub>Cp,m</sub>), 3.55 (s, 6 H, CH<sub>3,ester</sub>), 2.73 (m, 2 H, CH<sub>2,β</sub>), 2.52 (m, 2 H, CH<sub>2,β</sub>) ppm.  $^{13}\text{C}$  NMR ( $\text{CDCl}_3$ ):  $\delta$  = 173.4 (C=O<sub>ester</sub>), 170.3 (C=O<sub>amide</sub>), 144.6 (C<sub>q,ar</sub>), 129.7, 128.2, 127.0 (CH<sub>ar,Trt</sub>), 76.0 (C<sub>q,Cp</sub>), 72.2, 71.8, 70.8, 70.4 (CH<sub>Cp</sub>), 67.3 (C<sub>q,Trt</sub>), 53.1, 51.9 (CH<sub>α</sub> and CH<sub>3,ester</sub>), 33.5 (CH<sub>2,β</sub>) ppm.

**Fe[C<sub>5</sub>H<sub>4</sub>–CO–Cys(SH)–OMe]<sub>2</sub> (2):** Fe[C<sub>5</sub>H<sub>4</sub>–CO–Cys(Trt)–OMe]<sub>2</sub> (**1**; 1.0 mmol) was dissolved in TFA (30 mL) in a round-bottomed flask (100 mL), and a large excess of phenol (2.2 g) and TIS (triisopropylsilane, 1.0 mL) were added. The reaction mixture was subsequently stirred at ambient temperature under an inert atmosphere for 30 min. Solvents were removed by rotary evaporation, and the residue was chromatographed on silica gel (CH<sub>2</sub>Cl<sub>2</sub>/MeOH, 99:1) to yield **2** as an orange powder (325 mg, 64%). C<sub>20</sub>H<sub>24</sub>FeN<sub>2</sub>O<sub>6</sub>S<sub>2</sub> (508.39): calcd. C 47.25, H 4.76, N 5.51; found C 46.25, H 4.86, N 5.97. MS (EI):  $m/z$  = 509 [M + H]<sup>+</sup>. UV/Vis (CH<sub>2</sub>Cl<sub>2</sub>):  $\lambda$  ( $\epsilon$ , M<sup>-1</sup>cm<sup>-1</sup>) = 442.1 (249) nm.  $E_{1/2}$  = 398 mV (vs. Fc/Fc<sup>+</sup>). FTIR (KBr):  $\tilde{\nu}$  = 3294 (br. s, ν<sub>NH</sub>), 3080, 2962, 2863 (br. s, ν<sub>OH</sub> and ν<sub>CH,ar</sub>), 1752 (s, ν<sub>C=O,ester</sub>), 1654, 1628 (s, ν<sub>amide stretch</sub>), 1542 (s, ν<sub>amide bending</sub>) cm<sup>-1</sup>.  $^1\text{H}$  NMR ( $\text{CDCl}_3$ ):  $\delta$  = 7.55 (d,  $J_{\text{HH}}$  = 8.5 Hz, 2 H, NH), 5.14–5.06 (m, 2 H, CH<sub>α</sub>), 4.88 (m, 2 H, CH<sub>Cp,o</sub>), 4.79 (m, 2 H, CH<sub>Cp,o</sub>), 4.55 (m, 2 H, CH<sub>Cp,m</sub>), 4.42 (m, 2 H, CH<sub>Cp,m</sub>), 3.84 (s, 6 H, CH<sub>3,ester</sub>), 3.05–2.92 (m, 4 H, CH<sub>2,β</sub>) ppm (SH signals are missing, as they are obscured by solvent exchange).  $^{13}\text{C}$  NMR ( $\text{CDCl}_3$ ):  $\delta$  = 171.4 (C=O<sub>ester</sub>), other quart. C atoms were not observed, 71.0, 70.1, 68.7, 68.5 (CH<sub>Cp</sub>), 53.0 and 51.9 (CH<sub>α</sub> and CH<sub>3,ester</sub>), 41.3 (CH<sub>2,β</sub>) ppm.

**Fe[C<sub>5</sub>H<sub>4</sub>–CO–Cys–OMe]<sub>2</sub>[Fe<sub>3</sub>(CO)<sub>12</sub>] (3a):** A solution of Fe<sub>3</sub>(CO)<sub>12</sub> (100.7 mg, 0.2 mmol) in freshly distilled dry CHCl<sub>3</sub> (20 mL) was added dropwise under argon to a stirred suspension of Fe[C<sub>5</sub>H<sub>4</sub>–CO–Cys–OMe]<sub>2</sub> (**2**; 208 mg, 0.6 mmol) in dry MeOH (20 mL). The

mixture was heated under reflux for 90 min at 90 °C, which resulted in the formation of a dark-red solution. All volatiles were removed under reduced pressure, and the residue was triturated in cold MeOH and subsequently filtered to yield a dark-red solid. Compounds **3a** and **3b** were separated by column chromatography [EtOAc/hexane, 2:1;  $R_f$  = 0.2 for **3a**]. Yield = 245 mg (0.31 mmol, 52%). Single crystals of **3a** suitable for X-ray analysis were obtained from the slow evaporation of toluene from a toluene/heptane mixture. C<sub>26</sub>H<sub>22</sub>Fe<sub>3</sub>N<sub>2</sub>O<sub>12</sub>S<sub>2</sub> (786.13): calcd. C 40.39, H 3.00, N 3.62; found C 40.98, H 3.53, N 3.58. MS (FAB):  $m/z$  = 786.9 [M + H]<sup>+</sup>, 617.9 [M – 6 × CO]<sup>+</sup>. UV/Vis (CH<sub>2</sub>Cl<sub>2</sub>):  $\lambda_{\text{max}}$  ( $\epsilon$ , M<sup>-1</sup>cm<sup>-1</sup>) = 336 (9881), 450 (1638) nm. IR (KBr):  $\tilde{\nu}$  = 3327 (s, ν<sub>NH</sub>), 2930 (br. s), 2077, 2040, 2000 (s, ν<sub>Fe–C=O</sub>), 1743 (s, ν<sub>C=O,ester</sub>), 1659 (br. s, ν<sub>amide</sub>), 1512 (s, ν<sub>amide</sub>) cm<sup>-1</sup>.  $^1\text{H}$  NMR ( $\text{CDCl}_3$ ):  $\delta$  = 7.04 (d,  $J_{\text{HH}}$  = 6.9 Hz, 1 H, NH), 6.46 (d,  $J_{\text{HH}}$  = 7.2 Hz, 1 H, NH), 5.07 (m, 1 H, C<sub>α</sub>H), 4.85–4.77 (m, 3 H, CH<sub>α</sub> and CH<sub>Cp,o</sub>), 4.59–4.34 (m, 6 H, CH<sub>Cp,o</sub> and CH<sub>Cp,m</sub>), 3.94 (s, 3 H, CH<sub>3</sub>), 3.78 (s, 3 H, CH<sub>3</sub>), 3.21 (dd,  $J_{\text{HH}}$  = 4.7, 13.7 Hz, 1 H, C<sub>β</sub>H<sub>2</sub>), 2.98 (dd,  $J_{\text{HH}}$  = 3.0, 13.7 Hz, 1 H, C<sub>β</sub>H<sub>2</sub>), 2.80 (dd,  $J_{\text{HH}}$  = 5.1, 13.3 Hz, 1 H, C<sub>β</sub>H<sub>2</sub>), 2.54 (dd,  $J_{\text{HH}}$  = 3.2,  $J_{\text{HH}}$  = 13.3 Hz, 1 H, C<sub>β</sub>H<sub>2</sub>) ppm.  $^{13}\text{C}$  NMR ( $\text{CDCl}_3$ ):  $\delta$  = 207.7 (br., overlapping C=O<sub>Fe–CO</sub>), 170.0, 169.8, 169.6 (C=O<sub>ester</sub> and C=O<sub>amide</sub>), 79.5<sub>q</sub>, (C<sub>Cp</sub>), 72.0, 71.9, 71.8, 71.5, 71.4, 69.7, 68.8 (CH<sub>Cp</sub>), 53.3, 53.0, 52.8 (CH<sub>3</sub> and C<sub>α</sub>), 41.3, 25.0 (C<sub>β</sub>) ppm.

**Crystal data for 3a:** The crystal data was collected with a Bruker SMART-CCD diffractometer and the results were analyzed with the programs SHELXL-97 and SHELXS-97. Mo- $K_{\alpha}$  radiation ( $\lambda$  = 0.71073 Å). Flack parameter is 0.016(15), in agreement with the absolute configuration (L) of the amino acids used. Additional crystal and refinement data are summarized in Table 3.

Table 3. Crystal data and structure refinement for **3a**.

	<b>3a</b>
Chemical formula	C <sub>26</sub> H <sub>22</sub> Fe <sub>3</sub> N <sub>2</sub> O <sub>12</sub> S <sub>2</sub>
$M_r$ [g mol <sup>-1</sup> ]	786.13
Crystal system	Monoclinic
Space group	$P2_1$ (No.4)
$a$ [Å]	11.9081(8)
$b$ [Å]	9.9174(5)
$c$ [Å]	13.5225(9)
$\beta$ [°]	108.213(2)
$V$ [Å <sup>3</sup> ]	1516.97(16)
$Z$	2
$D_{\text{calcd.}}$ [g cm <sup>-3</sup> ]	1.721
Temperature [K]	153(2)
$2\theta_{\text{max}}$ [°]/total no. of reflections collected	54.32/18086
$\mu$ [mm <sup>-1</sup> ]	1.618
$R_1$ [ $I > 2\sigma(I)$ ] <sup>[a]</sup>	0.0454
$wR_2$ (all data) <sup>[b]</sup>	0.0739
Data/restraints/parameters	6048/1/406
GoF on $F^2$ <sup>[c]</sup>	1.050
Min./Max. res. density [e Å <sup>-3</sup> ]	0.585/–0.484
Flack parameter	0.016(15)

[a]  $R_1 = \sum ||F_o| - |F_c|| / \sum |F_o|$ . [b]  $wR_2 = \sum [w(F_o^2 - F_c^2)] / \sum [w(F_o^2)]^{1/2}$ , where  $w = 1 / \sigma^2(F_o^2) + (aP)^2 + bP$ ,  $P = (F_o^2 + 2F_c^2) / 3$ . [c] GoF =  $\{\sum [w(F_o^2 - F_c^2)^n - p]\}^{1/2}$  where  $n$  = no. of reflections and  $p$  = no. of refined parameters.

CCDC-663308 contains the supplementary crystallographic data for this paper. These data can be obtained free of charge from The Cambridge Crystallographic Data Centre via [www.ccdc.cam.ac.uk/data\\_request/cif](http://www.ccdc.cam.ac.uk/data_request/cif).

**Fe[C<sub>5</sub>H<sub>4</sub>CO-Cys(OMe)-S-S-Cys(OMe)-CO-C<sub>5</sub>H<sub>4</sub>] (3b):** Yield = 63 mg (0.13 mmol, 21%). C<sub>20</sub>H<sub>22</sub>FeN<sub>2</sub>O<sub>6</sub>S<sub>2</sub> (506.37): calcd. C 47.44, H 4.38, N 5.53; found C 47.54, H 5.06, N 5.08. MS (FAB): *m/z* = 506 [M]<sup>+</sup>. UV/Vis (CH<sub>2</sub>Cl<sub>2</sub>): λ<sub>max</sub> (ε, M<sup>-1</sup>cm<sup>-1</sup>) = 446 (259) nm. E<sub>1/2</sub> = 378 mV (vs. Fc/Fc<sup>+</sup>). FTIR (KBr): ν̄ = 3390, 3265 (s, ν<sub>NH</sub>), 2951 (s, ν<sub>CH,ar</sub>), 1749 (s, ν<sub>C=O,ester</sub>), 1663, 1644 (s, ν<sub>amide stretch</sub>), 1543 (s, ν<sub>amide bending</sub>) cm<sup>-1</sup>. <sup>1</sup>H NMR (CDCl<sub>3</sub>): δ = 7.34 (d, J<sub>HH</sub> = 7.0 Hz, 2 H, NH), 5.12 (dt, J<sub>HH</sub> = 4.7, 7.1 Hz, 2 H, CH<sub>α</sub>), 4.84 (m, 2 H, CH<sub>CP,o</sub>), 4.60–4.54 (m, 4 H, CH<sub>CP,o</sub> and CH<sub>CP,m</sub>), 4.44 (m, 2 H, CH<sub>CP,m</sub>), 3.80 (s, 6 H, CH<sub>3,ester</sub>), 3.49–3.34 (dd, J<sub>HH</sub> = 4.0, 10.1 Hz, 4 H, CH<sub>2,β</sub>) ppm. <sup>13</sup>C NMR (CD<sub>3</sub>OD): δ = 175.8 (C=O<sub>ester</sub>), 174.9 (C=O<sub>amide</sub>), 80.9 (C<sub>q,Cp</sub>), 78.5, 74.7, 73.9, 70.8 (CH<sub>CP</sub>), 55.0, 54.2 (CH<sub>α</sub> and CH<sub>3,ester</sub>), 48.3 (CH<sub>2,β</sub>) ppm.

## Acknowledgments

The authors are grateful to Dr. E. Bill for running the Mössbauer experiment and to Dr. Lehmann and his coworkers for the X-ray data acquisition. Dr. S. Kirin and Prof. Dr. H.-B. Kraatz have contributed through insightful discussions. Financial support during the initial phase of this project from the Deutsche Forschungsgemeinschaft (DFG) is gratefully acknowledged. X.d.H. performed a joint French–German PhD (Cotutelle de these).

- [1] M. Stephenson, L. H. Stickland, *Biochem. J.* **1931**, *25*, 205–214.
- [2] J. W. Peters, W. N. Lanzilotta, B. J. Lemon, L. C. Seefeldt, *Science* **1998**, *282*, 1853–1858.
- [3] Y. Nicolet, C. Piras, P. Legrand, C. E. Hatchikian, J. C. Fontecilla-Camps, *Structure* **1999**, *7*, 13–23.
- [4] A. Volbeda, M.-H. Charon, C. Piras, E. C. Hatchikian, M. Frey, J. C. Fontecilla-Camps, *Nature* **1995**, *373*, 580–587.
- [5] J. W. Tye, M. B. Hall, M. Y. Darensbourg, *Proc. Natl. Acad. Sci. USA* **2005**, *102*, 16911–16912.
- [6] R. H. Morris in *Concepts and Models in Bioinorganic Chemistry* (Eds.: H.-B. Kraatz, N. Metzler-Nolte), Wiley-VCH, Weinheim, **2006**, pp. 331–362.
- [7] A. C. Marr, D. J. E. Spencer, M. Schroder, *Coord. Chem. Rev.* **2001**, *219–221*, 1055–1074.
- [8] D. J. Evans, C. J. Pickett, *Chem. Soc. Rev.* **2003**, *32*, 268–275.
- [9] I. P. Georgakaki, M. Y. Darensbourg in *Comprehensive Coordination Chemistry II* (Eds.: L. Que Jr, W. B. Tolman), Elsevier, Amsterdam, **2003**, vol. 8, pp. 549–568.
- [10] L.-C. Song, J. Cheng, J. Yan, H.-T. Wang, X.-F. Liu, Q.-M. Hu, *Organometallics* **2006**, *25*, 1544–1547.
- [11] Y. Oudart, V. Artero, J. Pecaut, M. Fontecave, *Inorg. Chem.* **2006**, *45*, 4334–4336.
- [12] L. Schwartz, G. Eilers, L. Eriksson, A. Gogoll, R. Lomoth, S. Ott, *Chem. Commun.* **2006**, 520–522.
- [13] A. Perra, E. S. Davies, J. R. Hyde, Q. Wang, J. McMaster, M. Schroeder, *Chem. Commun.* **2006**, 1103–1105.
- [14] I. P. Georgakaki, L. M. Thomson, E. J. Lyon, M. B. Hall, M. Y. Darensbourg, *Coord. Chem. Rev.* **2003**, *238–239*, 255–266.
- [15] X. Liu, S. K. Ibrahim, C. Tard, C. J. Pickett, *Coord. Chem. Rev.* **2005**, *249*, 1641–1652.
- [16] L. Sun, B. Åkermark, S. Ott, *Coord. Chem. Rev.* **2005**, *249*, 1653–1663.
- [17] A. K. Justice, R. C. Linck, T. B. Rauchfuss, S. R. Wilson, *J. Am. Chem. Soc.* **2004**, *126*, 13214–13215.
- [18] J. I. v. d. Vlugt, T. B. Rauchfuss, C. M. Whaley, S. R. Wilson, *J. Am. Chem. Soc.* **2005**, *127*, 16012–16013.
- [19] S. Ezzaher, J.-F. Capon, F. Gloaguen, F. Y. Pétillon, P. Schollhammer, J. Talarmin, *Inorg. Chem.* **2007**, *46*, 3426–3428.
- [20] S. Ogo, R. Kabe, K. Uehara, B. Kure, T. Nishimura, S. C. Menon, R. Harada, S. Fukuzumi, Y. Higuchi, T. Ohhara, T. Tamada, R. Kuroki, *Science* **2007**, *316*, 585–587.
- [21] C. Mealli, T. B. Rauchfuss, *Angew. Chem. Int. Ed.* **2007**, *46*, 8942–8944.
- [22] T. Liu, M. Y. Darensbourg, *J. Am. Chem. Soc.* **2007**, *129*, 7008–7009.
- [23] D. Morvan, J.-F. Capon, F. Gloaguen, A. Le Goff, M. Marchivie, F. Michaud, P. Schollhammer, J. Talarmin, J.-J. Yaouanc, R. Pichon, N. Kervarec, *Organometallics* **2007**, *26*, 2042–2052.
- [24] L.-C. Song, M.-Y. Tang, F.-H. Su, Q.-M. Hu, *Angew. Chem. Int. Ed.* **2006**, *45*, 1130–1133.
- [25] J. Ekström, M. Abrahamsson, C. Olson, J. Bergquist, F. B. Kaynak, L. Eriksson, L. Sun, H.-C. Becker, B. Åkermark, L. Hammarström, S. Ott, *Dalton Trans.* **2006**, 4599–4606.
- [26] S. Ott, M. Kritikos, B. Åkermark, L. Sun, *Angew. Chem. Int. Ed.* **2003**, *42*, 3285–3288.
- [27] S. Ott, M. Borgström, M. Kritikos, R. Lomoth, J. Bergquist, B. Åkermark, L. Hammarström, L. Sun, *Inorg. Chem.* **2004**, *43*, 4683–4692.
- [28] C. Tard, X. Liu, S. K. Ibrahim, M. Bruschi, L. De Gioia, S. C. Davies, X. Yang, L.-S. Wang, G. Sawers, C. J. Pickett, *Nature* **2005**, *433*, 610–613.
- [29] C. He, M. Wang, X. Zhang, Z. Wang, C. Chen, J. Liu, B. Åkermark, L. Sun, *Angew. Chem. Int. Ed.* **2004**, *43*, 3571–3574.
- [30] X. de Hatten, T. Weyhermüller, N. Metzler-Nolte, *J. Organomet. Chem.* **2004**, *689*, 4856–4867.
- [31] S. Chowdhury, G. Schatte, H.-B. Kraatz, *Dalton Trans.* **2004**, 1726–1730.
- [32] A. V. Lesikar, *J. Chem. Phys.* **1964**, *40*, 2746.
- [33] R. M. G. Roberts, J. Silver, *J. Organomet. Chem.* **1984**, *263*, 235–241.
- [34] S. Shima, E. J. Lyon, R. K. Thauer, B. Mienert, E. Bill, *J. Am. Chem. Soc.* **2005**, *127*, 10430–10435.
- [35] L. Schwartz, J. Ekström, R. Lomoth, S. Ott, *Chem. Commun.* **2006**, 4206–4208.
- [36] A. Winter, L. Zsolnai, G. Huttner, *Z. Naturforsch., Teil B* **1982**, *37*, 1430–1436.
- [37] D. Seyferth, R. S. Henderson, *J. Organomet. Chem.* **1981**, *218*, C34–C36.
- [38] R. Happe, W. Rosenboom, A. J. Pierik, S. P. J. Albracht, K. A. Bagley, *Nature* **1997**, *385*, 126.
- [39] S. I. Kirin, H.-B. Kraatz, N. Metzler-Nolte, *Chem. Soc. Rev.* **2006**, *35*, 348–354.
- [40] S. I. Kirin, D. Wissenbach, N. Metzler-Nolte, *New J. Chem.* **2005**, *29*, 1168–1173.
- [41] S. I. Kirin, U. Schatzschneider, X. de Hatten, T. Weyhermüller, N. Metzler-Nolte, *J. Organomet. Chem.* **2006**, *691*, 3451–3457.
- [42] A. Volbeda, E. Garcin, C. Piras, A. L. de Lacey, V. M. Fernandez, E. C. Hatchikian, M. Frey, J. C. Fontecilla-Camps, *J. Am. Chem. Soc.* **1996**, *118*, 12989–12996.
- [43] N. J. Long, *Metallocenes: An Introduction to Sandwich Complexes*, Oxford, **1998**.
- [44] H.-B. Kraatz, J. Luszyk, G. D. Enright, *Inorg. Chem.* **1997**, *36*, 2400–2405.
- [45] C. Elschenbroich, A. Salzer, *Organometallics: A Concise Introduction*, Wiley-VCH, Weinheim, **1992**.
- [46] J. W. Peters, R. K. Szilagyi, A. Naumov, T. Douglas, *FEBS Lett.* **2006**, *580*, 363–367.
- [47] O. Pilak, B. Mamat, S. Vogt, C. H. Hagemeyer, R. K. Thauer, S. Shima, C. Vonrhein, E. Warkentin, U. Ermler, *J. Mol. Biol.* **2006**, *358*, 798–809.
- [48] M. R. Leach, D. B. Zamble, *Curr. Opin. Chem. Biol.* **2007**, *11*, 159–165.
- [49] H.-B. Kraatz, N. Metzler-Nolte (Eds.), *Concepts and Models in Bioinorganic Chemistry*, Wiley-VCH, Weinheim, **2006**.
- [50] I. Bertini, H. B. Gray, E. I. Stiefel, J. S. Valentine, *Biological Inorganic Chemistry: Structure and Reactivity*, University Science Books, Sausalito, California, **2007**.

- [51] S. J. Lippard, J. M. Berg, *Principles of Bioinorganic Chemistry*, University Science Books, Mill Valley, California, **1994**.
- [52] K. N. Green, S. P. Jeffery, J. H. Reibenspies, M. Y. Darzensbourg, *J. Am. Chem. Soc.* **2006**, *128*, 6493–6498.
- [53] C. E. Laplaza, R. H. Holm, *J. Am. Chem. Soc.* **2001**, *123*, 10255–10264.
- [54] A. L. Nivorozhkin, B. M. Segal, K. B. Musgrave, S. A. Kates, B. Hedman, K. O. Hodgson, R. H. Holm, *Inorg. Chem.* **2000**, *39*, 2306–2313.
- [55] C. E. Laplaza, R. H. Holm, *J. Biol. Inorg. Chem.* **2002**, *7*, 451–460.
- [56] K. B. Musgrave, C. E. Laplaza, R. H. Holm, B. Hedman, K. O. Hodgson, *J. Am. Chem. Soc.* **2002**, *124*, 3083–3092.
- [57] J. J. Pastuszak, A. Chimiak, *J. Org. Chem.* **1981**, *46*, 1868–1873.
- [58] D. R. van Staveren, T. Weyhermüller, N. Metzler-Nolte, *Dalton Trans.* **2003**, 210–220.

Received: June 4, 2008  
Published Online: August 29, 2008